Geoderma 390 (2021) 114948

Contents lists available at ScienceDirect

Geoderma

journal homepage: www.elsevier.com/locate/geoderma

Changes in pore networks and readily dispersible soil following structure liming of clay soils

Tobias Bölscher [a,b,*], John Koestel [a,c], Ararso Etana [a], Barbro Ulén [a], Kerstin Berglund [a], Mats Larsbo [a,*]

[a] Department of Soil and Environment, Swedish University of Agricultural Sciences, P.O. Box 7014, SE-750 07 Uppsala, Sweden
[b] Department of Biology, Lund University, Sölvegatan 37, SE-223 62 Lund, Sweden
[c] Soil Quality and Soil Use, Agroscope, Reckenholzstrasse 191, CH-8046 Zürich, Switzerland

ARTICLE INFO

Handling Editor: Yvan Capowiez

Keywords:
Soil structure, Structure liming
Pore space
Dispersible clay
X-ray computed tomography

ABSTRACT

Structure liming aims to improve soil structure (i.e., the spatial arrangement of particles and pores) and its stability against external and internal forces. Effects of lime application on soil structure have received considerable interest, but only a few studies have investigated effects on macro- and mesopore networks. We used X-ray computed tomography to image macropore networks (ø ≥ 0.3 mm) in soil columns and mesopores (ø ≥ 0.01 mm) in soil aggregates from three field sites with (silty) clay soils after the application of structure lime (3.1 t ha^{-1} or 5 t ha^{-1} of CaO equivalent). Segmented X-ray images were used to quantify soil porosity and pore size distributions as well as to analyse pore architecture and connectivity metrics. In addition, we investigated the amount of readily dispersible soil particles. Our results demonstrate that structure liming affected both, macropore networks and amounts of readily dispersible soil to different degrees, depending on the field site. Significant changes in macropore networks and amounts of readily dispersible soil after lime application were found for one of the three field sites, while only some indications for similar changes were observed at the other two sites. Overall, structure liming tended to decrease soil macroporosity and shift pore size distribution from larger ($\varepsilon_{>1.0\ mm}$) and medium sized macropores ($\varepsilon_{0.3–1.0\ mm}$) towards smaller macropores ($\varepsilon_{0.1–0.3\ mm}$). Furthermore, liming tended to decrease the critical and average pore diameters, while increasing the surface fractal dimension and specific surface area of macropore network. Structure liming also reduced the amounts of readily dispersible soil particles. We did not find any changes in mesopore network properties within soil aggregates or biopore networks in columns and aggregates. The effects of lime on macropore networks remain elusive, but may be caused by the formation of hydrate phases and carbonates which occupy pore space.

1. Introduction

Soil liming is a widespread agricultural practice commonly employed to increase pH in acidic soils and thereby increase crop yields. Any lime application can, however, alter an array of additional biological, chemical, and physical soil properties (Haynes and Naidu, 1998; Holland et al., 2018). It is therefore used to improve soil functioning, both, in general and for improving soil structure and structure stability (Bronick and Lal, 2005; Haynes and Naidu, 1998; Holland et al., 2018). In the latter cases, quicklime CaO or hydrated quicklime $Ca(OH)_2$ (both referred to as structure lime) are mainly used (Berglund, 1971; Keiblinger et al., 2016; Wiklander, 1963), because effects of calcium carbonate ($CaCO_3$) on soil structure are limited (Berglund, 1971; Choquette et al., 1987). Soil structure refers to the spatial arrangement of particles and pores within soils, while structural stability refers to the ability of a soil to retain its structure when exposed to internal (e.g. water flow) or external (e.g. field traffic) forces (Dexter, 1988). Soil structure controls aeration, hydraulic properties and leaching of substances. Recently, it has been suggested that lime application may reduce phosphorus leaching from clay soils (Svanbäck et al., 2014; Ulén et al., 2012; Ulén and Etana, 2014), when phosphorus transport through the soil is predominantly occurring attached to colloids through preferential flow paths (Svanbäck et al., 2014; Ulén et al., 2012). Reductions in phosphorus leaching may be an effect of (i) liming induced changes in

* Corresponding authors at: Stockbridge School of Agriculture, University of Massachusetts Amherst, 161 Holdsworth Way, Amherst, MA 01003, USA (Tobias Bölscher).
E-mail addresses: Tobias.Bolscher@biol.lu.se (T. Bölscher), Mats.Larsbo@slu.se (M. Larsbo).

https://doi.org/10.1016/j.geoderma.2021.114948
Received 10 September 2020; Received in revised form 15 January 2021; Accepted 17 January 2021
Available online 12 February 2021

soil structure, e.g. a lower susceptibility to preferential flow, and/or (ii) a decrease in readily dispersible soil (see section 2.4) caused by the stabilizing effects of structure lime, which results in reduced particle transport.

The structure of clay soils and their stability may be influenced by lime application via several direct and indirect processes. For instance, lime application introduces additional Ca^{2+} ions into the soil solution and thereby increases the ionic strength, which favours flocculation of phyllosilicate clays and particles holding negatively charged functional groups. This flocculation can rearrange soil particles and contribute to the formation of aggregates. Lime induced flocculation may therefore reshape soil pore networks (Haynes and Naidu, 1998; Holland et al., 2018). Lime application may also trigger the formation of hydrate phases and carbonates which form in the pore space and can clog connections between pore clusters (Witt, 2002; Zimmermann et al., 2016). Indirectly, liming may change soil structure via increased soil pH which stimulates root growth and earthworm activity. Both of these processes are important for the formation of macropores. A stimulated biological activity may further improve structural stability through the formation of stable aggregates. Earthworms glue soil particles together through their ingestion and excretion of particles. Fungi and fine roots connect micro-aggregates together to macro-aggregates, while fungal and bacterial excretions have gluing properties (Haynes and Naidu, 1998; Holland et al., 2018).

Effects of liming on soil structure have attracted considerable interest (e.g. Anikwe et al., 2016; Auler et al., 2017; Carmeis Filho et al., 2016; Chan et al., 2007; Grieve et al., 2005; Shanmuganathan and Oades, 1983), but only a limited number of studies have investigated related changes in pore networks. These studies have focused on subtropical or tropical soils and mainly used traditional analytical techniques (e.g. deriving porosities from bulk density and/or water retention data; Anikwe et al., 2016; Auler et al., 2017; Rodrigues da Silva et al., 2016) which yield only indirect information about the architecture of pore networks. During the last decades, X-ray computed tomography (CT) has emerged as an important tool to investigate soil structure and pore architecture via 3D image analysis. It provides direct information about pore networks and their geometrical properties such as shape and connectivity (Helliwell et al., 2013). Although X-ray CT has become a standard tool in soil physics research, only few studies have used this technique to investigate effects of liming on pore networks in agricultural soils (Ferreira et al., 2019, 2018; Hellner et al., 2018; Nunes et al., 2018).

Two studies investigated subtropical soil. Nunes et al. (2018) analysed pore structures in repacked soil from an Oxisol one year after lime incorporation. High doses of lime ($\geq$7.8 t ha^{-1}, lime type not specified) decreased the amount of larger pores (1–2.5 mm), the pore surface area, and the pore connectivity in the layer below lime incorporation. These changes were likely due to pore filling and migration of clay sized particles, because clay dispersed when Ca^{2+} substituted Al^{3+} in this highly weathered soil (Nunes et al., 2018). Ferreira et al. (2018) investigated a no-till field 30 month after surface lime application (20 t ha^{-1} CaO). Liming resulted only in small changes in pore architecture, but the upper layer (0–10 cm) of limed soil tended to have higher porosity and better connectivity compared to the lower layer (10–20 cm). Non-limed soil showed no such trend (Ferreira et al., 2018). Both above mentioned studies investigated a single soil with a limited number of replicates (n = 4 and 3 for Nunes et al., 2018; Ferreira et al., 2018, respectively). Due to differences in soil properties between subtropical and temperate soils, findings from these studies may not apply for clay soils in Sweden. Hellner et al. (2018) used intact soil columns (18.0 cm high, 12.7 cm diameter, n = 8) from conventionally tilled limed and control plots on a silty clay field in Sweden. Structure lime in the form of quicklime (5 t ha^{-1} CaO) had been applied 7 years prior to sampling. They did not detect any differences in pore network properties between limed and control plots and suggested that the impact of liming on pore network properties may have been limited to pores smaller than the size that could be resolved in their X-ray images (i.e. 325 μm). They further argued that liming effects on soil structure may have been limited to a few years after lime application and had diminished by the time of analysis (Hellner et al., 2018). In summary, results from previous studies using X-ray CT images do not give a clear picture on how liming affects soil structure. The partly opposing results may have been caused by differences in soil type, different amount and type of lime used, diminished effects of liming over time, limited number of samples, and poor image resolution.

Early studies investigating liming effects on soil structure stability (e.g. wet aggregate stability) and clay dispersion show contrasting results, which may be due to different periods of time between lime application and analyses (Haynes and Naidu, 1998): Clay dispersion may initially increase for a few months as an effect of raised soil pH in acidic soils. In these soils, lime application can cause short-term repulsive forces between clay particles. In the longer perspective structure stability was, however, generally improved due to clay flocculation, the cementing effects of $CaCO_3$, and effects of increased pH on root growth and microbiology (Haynes and Naidu, 1998). More recently, Blomquist et al. (2018) showed that clay dispersion was significantly reduced for clay soils treated with 4.2 t Ca ha^{-1} applied as $Ca(OH)_2$ or a mixture of $Ca(OH)_2$ and $CaCO_3$. Lime application with lower doses showed no significant effects on clay dispersion (Blomquist et al., 2018). Ulén and Etana (2014) also found reduced clay dispersion in soils treated with lime for two field experiments on soils with around 60% and 25% clay content, treated with 5 t ha^{-1} CaO and 2.8 t ha^{-1} $Ca(OH)_2$, respectively. The lime had been applied three and two years prior to the studies, respectively. Soil dispersion may thus be reduced on a longer perspective by liming if sufficient amounts of lime are applied, with effects lasting for at least two to three years.

The aim of the present study was to quantify effects of lime application on pore networks and readily dispersible soil of (silty) clay soils (clay content >45%). Therefore, we sampled intact soil columns and soil aggregates from three Swedish field experiments to which two types of structure lime (CaO and a mixture of $Ca(OH)_2$ and $CaCO_3$) had been applied two or nine years earlier. We studied pore networks using X-ray CT and measured amounts of readily dispersible soil after wet sieving. We hypothesized that liming would alter soil porosity and pore network properties, but left the direction of the change open, because potentially involved mechanisms may work in different directions (Haynes and Naidu, 1998; Holland et al., 2018). We further expected that lime application would reduce the amounts of readily dispersible soil.

2. Material and methods

2.1. Field sites

We sampled three experimental fields with (silty) clay soils in mid-eastern Sweden. The field sites Ultuna 3 and Ultuna 9 (i.e. sub-sites no. 3 and 9 of the Ultuna experimental field site) are located close to each other approx. 5 km south of Uppsala (59°48'N, 17°39'E) and Oxelby is located close to Lake Bornsjön, approx. 20 km south-west of Stockholm (59°14'N, 17°40'E).

The Ultuna experiments were established in October 2014 using a randomized block design (12 m × 20 m plots replicated four times). Soils were Eutric Cambisols (FAO, 1998) with a silty clay to clay texture containing around 50% clay (pipette method; Gee and Or, 2002) and a slightly to moderately acidic pH ($CaCl_2$, Table 1). The dominant clay mineral is illite (Wiklander and Lotse, 1966). The limed plots received 6 t ha^{-1} of a commercial lime powder mixture (calcium content equivalent to approx. 3 t ha^{-1} CaO, Nordkalk Aktive Struktur) containing slaked lime (approx. 20%) and ground lime stone. The lime mixture was incorporated into the upper 15 cm using a tine cultivator and control plots received no lime application. Under the trial period (i.e. 2014–2017), the soil was managed with a non-inversion tine cultivator and spring barley was grown. Long-term mean annual temperature and

Table 1
Soil texture, texture class (USDA), total organic carbon (C org.), years since structure liming (yr) and soil pH at the three investigated field sites. Values were determined at selected plots representing the entire field site (Berglund et al., 2017; Hellner et al., 2018), except for soil pH for which values represent means for limed and control plots (n = 12); *p < 0.05, **p < 0.01, ***p < 0.001.

Site	Texture class	Clay (%)	Silt (%)	Sand (%)	C org. (%)	Yr	Treatment	pH ($CaCl_2$)
Ultuna 3	Silty clay	46	40	15	2.8	3	limed	6.7 ***
							control	6.0
Ultuna 9	Clay	57	36	7	4.1	3	limed	6.7 ***
							control	5.6
Oxelby	Silty clay	47	48	5	2.1	10	limed	6.0 ***
							control	5.4

precipitation recorded at a nearby climate station are 5.5 °C and 572 mm, respectively (Sandin et al., 2017).

The Oxelby trial was established in September 2007. Limed plots and control plots are arranged in a randomized block design (20 m × 24 m plots replicated four times; Svanbäck et al., 2014; Ulén et al., 2012). The soil is a Eutric Cambisol (FAO, 1998; Ulén and Persson, 1999) with a silty clay texture containing around 48% clay (pipette method; Gee and Or, 2002) dominated by expandable phyllosilicates with high charges (i.e. 80–90% of the phyllosilicates are vermiculitic; M. Simonsson, SLU, *personal communication*). The soil pH is strongly to moderately acidic (Table 1). Limed plots received 5 t ha^{-1} CaO which was incorporated into the top soil to about 10 cm using a cultivator while control plots received no lime. In the years following lime application, the soils were conventionally ploughed using a mouldboard plough. Spring crops were sown following a four-year rotation scheme with twice barley (*Hordeum vulgare*), oats (*Avena sativa*) and peas (*Pisum sativum* subsp. *arvense*; Svanbäck et al., 2014). Average annual temperature and precipitation measured nearby the field are 6.8 °C and 525 mm, respectively (Climate-Data.org, 2020).

2.2. Soil sampling

Intact soil columns were sampled in September 2016 from a depth of approx. 6–13 cm using PVC cylinders (68 mm inner diameter, 70 mm height). Three cylinder samples were taken from each limed and control plot leading to 12 cylinders per treatment from each site (72 cylinders in total: 3 field sites × 2 treatments × 4 replicated plots × 3 cylinders). The sample cylinders were sealed and stored at 3 °C to avoid drying and limit biological activity for approx. three months until they were X-rayed. The aggregates were sampled in September 2017 by taking intact soil columns using steel cylinders (70 mm inner diameter, 100 mm height), following the procedure described above. In the laboratory, the samples were allowed to dry until the soil could be carefully pushed out of the cylinders. Aggregates with a diameter of approx. 5 mm were obtained by gently crushing the soil columns manually, ensuring breakage along natural planes of weakness (Ananyeva et al., 2013). Afterwards, the aggregates were air-dried and X-rayed within one month after sampling.

The samples for analysis of readily dispersible soil were collected in autumn 2018. Soil clods were taken from a depth of 3–8 cm with a shovel after removing vegetation at five randomly chosen locations in each plot. Approximately 2 kg soil per plot was collected in PVC boxes, which then were sealed and stored at 3 °C to avoid drying prior to analysis.

2.3. Soil structure analysis by 3D-imaging of macro- and mesopore networks

2.3.1. X-ray tomography

The soil columns and aggregates were scanned using a GE Phoenix v|tome|x m industrial X-ray scanner (GE Inspection Technologies, Lewistown, PA, USA). The scans of the soil columns were performed taking 1900 radiographs per sample with a voltage of 120 kV and a current of 390 μA. The exposure time for each radiograph was 200 μs and the pixel size 50 μm in both directions. The soil aggregates were placed inside an aluminium cylinder (8 mm inner diameter, 15 mm high) on a carbon fibre stick and 2000 radiographs per sample were collected with a voltage of 90 kV and a current of 60 μA. The exposure time for each radiograph was 200 μs and the pixel size was 5.5 μm in both directions The GE software datos|x (version 2.2, 2012) was used to reconstruct 3D images from the radiographs and the resulting 3D images were then exported as 16-bit grayscale TIFF-stacks. Considering the pixel sizes, scans of soil columns deliver information on macropore networks (Ø ≥0.1 mm) and scans of aggregates give information on mesopore networks (Ø ≥0.01 mm).

2.3.2. Image processing

We processed the image data using the Fiji distribution (Schindelin et al., 2012) of the open access software ImageJ (Schneider et al., 2012) and the ImageJ plug-in SoilJ (Koestel, 2018). Unless otherwise stated, default parameter settings were used for all processing steps.

The images of the soil columns were processed following the procedure outlined by Koestel (2018). In short, a 3D median filter with a 2-voxel radius was applied to reduce image noise and an unsharp mask filter with a 2-voxel standard deviation and a filter weight of 0.6 was used to enhance the sharpness of feature edges. Afterwards, the grey values were calibrated in all 3-D images to ensure that objects of the same density had the same grey values. The mean grey values of the PVC cylinder wall and the 0.1 percentile grey-value inside the columns (corresponding to air-filled pores) were used as reference values. All other grey values were scaled following a linear relation between reference values and initial grey values (Koestel and Larsbo, 2014). We segmented the images using the minimum error method (Kittler and Illingworth, 1986) applied to the joint histogram of grey values for all images. This segmentation separated mineral phases (assigned grey value 0) from particulate organic matter (POM) and pore-space (assigned grey value 255). The POM phase was then separated from the pore space by applying the segmentation method described in (Koestel and Schlüter, 2019), which uses the 2D histograms of the calibrated grey-scale images and the gradient images. Finally, the top and bottom surfaces of the soil columns were detected using SoilJ's standard routine (Koestel, 2018).

Soil aggregate images were generally processed in the same way as the soil column images, except that the aluminium cylinders values were used to define the upper reference value during the grey value calibration and that the images were segmented using the minimum grey-value (Prewitt and Mendelsohn, 1966) between the joint histogram peaks corresponding to air and soil matrix as a threshold. Further, the aggregate images required the detection of aggregate boundaries prior to analysis of pore networks, because pores with connections to the aggregate surface needed to be separated from the surrounding air. Otherwise, some pores may have been misclassified as surrounding air which may have substantially affected the results of the pore network analysis (Fig. 1a and b; Wang et al., 2012). To seal off the surface connected pores, we modified the two-step procedure described by Wang et al. (2012) and implemented it as a new tool (i.e., function 'Create Closing Mask') in the SoilJ plugin (version 1.1.4, 2017, and following). Our modified procedure is based on dilations followed by erosions on the solid phase. Choosing the number of dilations and erosions is a trade-

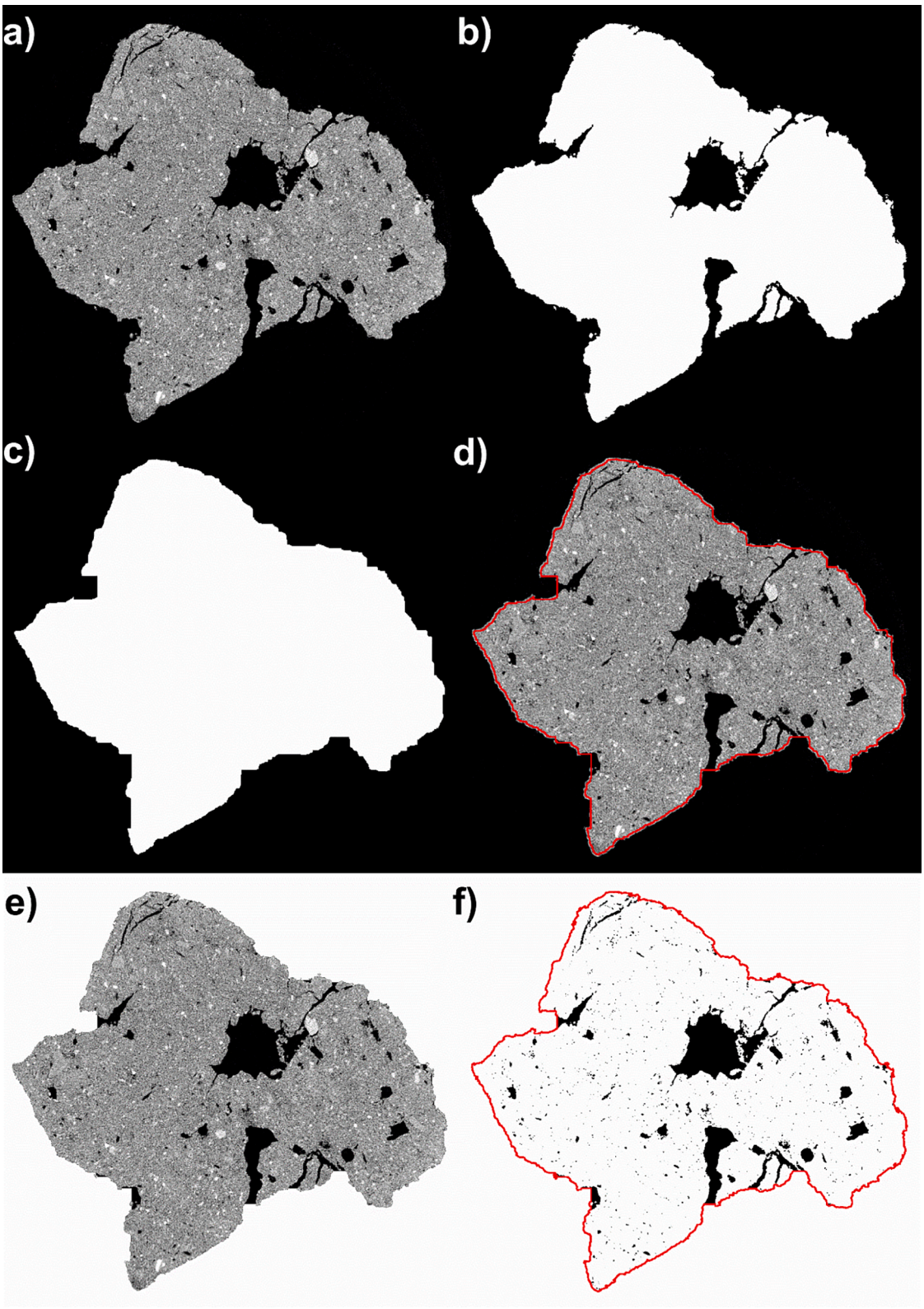

Fig. 1. Illustration of the three-step procedure to detect soil aggregate boundaries and to seal off surface connected pores during image analyses: a) Example of an unprocessed 2D grayscale image. b) The same image after segmentation (solid phase in white) showing large surface connected pores which were recognized as surrounding air (illustrated in black). c) The same image after 20 dilation steps followed by 26 erosion steps on the solid phase giving the preliminary aggregate mask; a region of interest (ROI) is delineated in red. d) Zoom into the ROI showing the original aggregate boundary (grey) and the overlaid preliminary aggregate mask (red). The preliminary aggregate mask is smaller than the original scan to minimize the creation of artefact pores at surface dents. e) The ROI showing the aggregate outline after combining the preliminary aggregate mask with the original aggregate boundaries (pores in black, surrounding air in white, solid phase in grey). It can be seen that artifacts from assigning surface dents as pore space are kept to a minimum. f) Final segmented aggregate image with the aggregate boundary in red, the pore space in black, and the mineral phase within the aggregate in white and the surrounding air outside the aggregate also in white.

Table 2
Probability (p) values for any differences in macropore networks (soil columns), mesopore networks (soil aggregates) and readily dispersible soil from structure limed and control plots. The direction of change due to liming (+ or –) and p-values are given in bold when differences are significant ($p < 0.05$).

		p values and direction of change		
Parameter		Ultuna 3	Ultuna 9	Oxelby
Macropore networks (soil columns)				
Total imaged porosity	ε_{tot}	**–0.021**	0.697	0.100
Absolute pore size distribution	$\varepsilon_{>1.0\ mm}$	**–0.004**	0.585	0.312
	$\varepsilon_{0.3–1.0\ mm}$	0.423	0.860	**–0.036**
	$\varepsilon_{0.1–0.3\ mm}$	0.058	**+0.006**	0.679
Relative pore size distribution	$\varepsilon_{>1.0\ mm}$	**–0.002**	0.914	0.487
	$\varepsilon_{0.3–1.0\ mm}$	**+0.005**	0.960	0.417
	$\varepsilon_{0.1–0.3\ mm}$	**+0.003**	0.734	0.074
Average pore diameter	d_{aver}	**–0.015**	0.947	0.934
Critical pore diameter	d_{crit}	**–0.040**	0.525	0.470
Connection probability	Γ	0.100	0.835	0.065
Percolating porosity	ε_p	0.100	0.471	0.179
Surface fractal dimension		0.078	**+0.000**	**+0.045**
Specific surface area		**+0.004**	0.946	0.059
Total imaged bioporosity	ε_{bio}	0.278	0.110	0.954
Absolute biopore size distribution	$\varepsilon_{bio\ >2.0\ mm}$	0.172	0.564	0.606
	$\varepsilon_{bio\ 1.0–2.0\ mm}$	0.274	0.866	0.115
	$\varepsilon_{bio\ 0.5–1.0\ mm}$	0.279	0.374	0.845
	$\varepsilon_{bio\ 0.1–0.5\ mm}$	0.677	0.967	0.814
Mesopore networks (soil aggregates)				
Total imaged porosity	ε_{tot}	0.830	0.431	0.538
Absolute pore size distribution	$\varepsilon_{>0.1\ mm}$	0.582	0.546	0.813
	$\varepsilon_{0.03–0.1\ mm}$	0.994	0.161	0.755
	$\varepsilon_{0.01–0.03\ mm}$	0.263	0.989	0.839
Relative pore size distribution	$\varepsilon_{>0.1\ mm}$	0.645	0.913	0.745
	$\varepsilon_{0.03–0.1\ mm}$	0.893	0.869	0.846
	$\varepsilon_{0.01–0.03\ mm}$	0.756	0.784	0.914
Average pore diameter	d_{aver}	0.785	0.644	0.780
Connection probability	Γ	0.623	0.656	0.326
Surface fractal dimension		0.537	0.123	0.294
Specific surface area		0.518	0.954	0.519
Total imaged bioporosity	ε_{bio}	0.782	0.578	0.316
Absolute biopore size distribution	$\varepsilon_{bio\ >2.0\ mm}$	0.160	0.687	0.616
	$\varepsilon_{bio\ 1.0–2.0\ mm}$	0.294	0.719	0.185
	$\varepsilon_{bio\ 0.5–1.0\ mm}$	0.280	0.315	0.828
	$\varepsilon_{bio\ 0.1–0.5\ mm}$	0.677	0.967	0.814
Readily dispersible soil				
Total readily dispersible soil	RDS_{tot}	**–0.040**	0.085	0.888
Readily dispersible clay	RDS_{clay}	**–0.050**	0.176	0.164
Readily dispersible soil larger than clay	$RDS_{>clay}$	**–0.038**	0.069	0.100

off between excluding surface connected pores with a relatively large diameter and introducing artefacts. A higher number of dilation and erosion steps closes larger surface connected pores, while air close to the aggregate surface may be incorrectly labelled as pore space due to surface dents and niches (Wang et al., 2012). To reduce the effects of this trade-off, we used a three-step procedure (Fig. 1): In a first step, surface connected pores were closed using 20 consecutive dilation steps. Each dilation step was conducted with a spherical kernel of 3 voxels in diameter. Then all 'holes', i.e. pores inside the aggregate were filled. This ensured that relatively large pores were sealed. In a second step, images were eroded using an erosion overshoot factor of 1.3 (i.e., 26 erosion steps) creating an aggregate mask with a smaller size than the original aggregates (Fig. 1c and d). Finally, this preliminary aggregate mask was combined with the initial segmented image using the logical OR operator to create the final aggregate mask (Fig. 1e and f). With this procedure, we could seal relatively large surface connected pores while minimizing the number of voxels incorrectly added to the surface. The created aggregate mask was then applied to the segmented binary images with the logical AND operator, leaving only the intra-aggregate pore network (Fig. 1f).

2.3.3. Image analysis

For the column samples, the analyses of imaged pore networks were performed on a centrally located cylindrical region of interest (ROI). Each ROI had a volume of 31.2 cm^3. The top was set at 500 voxels (i.e. 2.5 cm) below the detected mean elevation of the soil surface and the sides at a distance of 300 voxels (i.e. 1.5 cm) from the cylinder wall. The depth of each ROI was 550 voxels (i.e. 2.75 cm). We chose the described ROIs to minimize effects of sampling artefacts along cylinder walls. For the aggregates, the entire aggregate images were used in the analysis of mesopore networks. The introduction of systematic errors by analysing the entire aggregate is unlikely because there were no significant differences in aggregate volumes between treatments for any of the sites (Table 2). Similar procedures for pore network analyses were implemented for soil column ROIs and soil aggregates using the Pore Space Analyzer in SoilJ (Koestel, 2018), which also implements standard ImageJ and Fiji methods as well as routines included in the plugins BoneJ (Doube et al., 2010) and MorphoLibJ (Legland et al., 2016). However, parameters that require knowledge about *in-situ* orientation of pore networks (i.e., critical pore diameter and percolating porosity) were not analysed on soil aggregates, because the original orientation of the aggregates in the soil was not known due to the sampling procedure. The total imaged porosity ε_{tot} ($mm^3\ mm^{-3}$) was extracted by calculating the number of voxels with an assigned grey value of 255 from the segmented binary images. The specific surface area of the imaged pores was calculated from the total surface area and the total pore volume. The former was computed using the Crofton equation, implemented in MorphoLibJ (Legland et al., 2016). The average pore diameter d_{aver}

(mm) was quantified using the method of the largest inscribable sphere (Dougherty and Kunzelmann, 2007). From the distribution of pore diameters in the soil column ROIs, three volume fractions of imaged pores were calculated, namely with diameters between 0.1 and 0.3 mm ($\varepsilon_{0.1–0.3\ mm}$), between 0.3 and 1.0 mm ($\varepsilon_{0.3–1.0\ mm}$), and >1.0 mm ($\varepsilon_{>1.0\ mm}$). For the soil aggregates we evaluated the following three pore size classes: diameters between 0.01 and 0.03 mm ($\varepsilon_{0.01–0.03\ mm}$), between 0.03 and 0.1 mm ($\varepsilon_{0.03–0.1\ mm}$), and >0.1 mm ($\varepsilon_{>0.1\ mm}$). The critical pore diameter, d_{crit} (mm), the connection probability Γ (-) and the percolating porosity ε_p (%) were calculated using SoilJ routines. The critical pore diameter d_{crit} refers to the bottleneck pore diameter in the pore network connection from the top to the bottom of the ROI. The connection probability Γ quantifies the likelihood that two randomly chosen pore voxels belong to the same pore cluster (Renard and Allard, 2013). The percolating porosity ε_p refers to all imaged pore voxels with a connection to the top and the bottom of the ROI. The surface fractal dimension was calculated by the box counting method (Perret et al., 2003) implemented in SoilJ (Koestel, 2018). The surface fractal dimension is defined as the negative log–log slope between the number of voxels located at the interface of pores and non-pores and the voxel size for different image resolutions.

We segmented pores originating from biological activity using an approach that follows the method suggested in Lucas et al. (2019). In short, the biopores were defined as all pores that were approximately tube-shaped. In practice, we labelled all pore voxels as biopores, for which the tubeness measure implemented in ImageJ (Longair et al., 2017) had values larger than an ad-hoc threshold value of 60. The tubeness is the root of the product of the two largest eigenvalues (if they are both negative) of the Hessian of a blurred image. The blurring is applied by a Gaussian blur filter. The larger its footprint, the larger are the structures that are analysed. In our case we calculated the tubeness measure for Gaussian blur radii of 1, 2, 4, 8, 12, 16, 24, 32, 44 and 60 voxels. A voxel was considered to be part of a biopore if its tubeness score exceeded the threshold for at least one of the considered radii. Due to the surface roughness of the biopores, often only their medial axis is detected. Therefore, similar to Lucas et al. (2019), the identified biopores were dilated to approximate their volume. In this study, we set the number of dilations to the size of the radius used for the tubeness measurement. In the following, we refer to the volume fraction of the biopores, denoted as total imaged bioporosity (ε_{bio}) and four fractions of imaged biopores with diameters between 0.1 and 0.5 mm ($\varepsilon_{bio\ 0.1–0.5\ mm}$), between 0.5 and 1.0 mm ($\varepsilon_{bio\ 0.5–1.0\ mm}$), between 1.0 and 2.0 mm ($\varepsilon_{bio\ 1.0–2.0\ mm}$, and>2.0 mm ($\varepsilon_{bio\ >2.0\ mm}$).

2.4. Readily dispersible soil

Readily dispersible soil was quantified with a modification of the method by Czyż and Dexter (2015) after submerging aggregates in water and by using turbidity as an indicator of the amount of suspended soil particles. The field-moist soil clods were gently broken and sieved to collect aggregates of 8–11 mm size. Aggregates were placed in cups of a wet sieving apparatus (Eijkelkamp Soil & Water, Giesbeek, The Netherlands) with 250 μm sieves at the bottom. Each cup was holding 6 g soil, usually corresponding to 8 aggregates. The cups were then immersed in 80 mL distilled water (contained in stainless steel cylinders) by gently raising and lowering the cups for three minutes with an oscillation speed of 36 cycles min^{-1} (Almajmaie et al., 2017). Afterwards, aggregates remaining in the cups were discarded and the water samples from two cylinders (i.e.160 mL) were pooled, transferred to a plastic bottle (250 mL), and topped up with distilled water to a volume of 250 mL. For each replicated field plot, four such samples were prepared (i.e. n = 16). The water samples were then shaken for 10 min (90 revolutions min^{-1}) and turbidity was measured using a turbidimeter (2100 N, Hach Lange, Düsseldorf, Germany) two times, once directly after shaking ($turbidity_{0h}$) and a second time after sedimentation for 4.5 h ($turbidity_{4.5h}$). $Turbidity_{0h}$ was supposed to show suspension of clay, larger soil particles and fine aggregates, while $turbidity_{4.5h}$ was expected to represent the suspension of only clay particles (Sheldrick and Wang, 1993). We here define the former as total readily dispersible soil (RDS_{tot}) and the latter as readily dispersible clay (RDS_{clay}), while the difference between $turbidity_{0h}$ and $turbidit_{4.5h}$ represents the readily dispersible soil particles larger than the clay size fraction ($RDS_{>clay}$).

2.5. Soil pH

Soil pH was determined in 0.01 M $CaCl_2$ solution (1:5 w/v) on remaining, air-dried soil from the same soil columns as the aggregates used for imaging (i.e. 3 samples of mixed soil per plot). Before the measurement, all visually detectable roots and plant material were removed, and the samples were ground using a ball mill (MM2, Retsch, Haan, Germany).

2.6. Statistical analyses

Statistical analyses were carried out in Minitab 17 (2014; Minitab Ltd., Coventry, UK) testing for differences between structural limed and control plots at individual field sites. The data were analysed by fitting general linear models with treatment and block as fixed factors followed by Tukey's multiple comparison test, with a p-value <0.05 indicating statistical significance. Prior to the analyses, all data were tested for normality using the Anderson-Darling test and for equal variance using Levene's test. Where necessary, the data were log-transformed to obtain approximately normally distributed data with equal variances. The data for percolating porosity were neither normally distributed nor could they be successfully transformed. The reason for this was that for a considerable number of samples the percolating porosity was 0%. Therefore, we applied the Friedman test by ranks for these data.

3. Results

3.1. Soil pH

The incorporation of lime into the topsoil significantly increased soil pH at each of the three field trials (Table 1). At Ultuna 3 and Ultuna 9 pH values were 0.7 and 1.1 units higher in limed compared to control soils three years after liming, respectively. At Oxelby, soil pH was 0.6 units higher in limed compared to control treatments ten years after liming.

3.2. Macropore networks in soil columns

The effects of liming on macropore networks in soil columns differed between sites. We found most of the significant differences between limed and non-limed treatments in Ultuna 3 (Figs. 2–4, Table 2). Results from Ultuna 9 and Oxelby showed less significant effects (Figs. 2–4, Table 2). Whenever liming affected pore networks differences were consistent across field sites and pointed in the same direction (Figs. 2–4). A limited number of block effects ($p < 0.05$) were present at Ultuna 3 and Ultuna 9. These block effects were due to gradients in soil texture across field sites and are not further reported.

3.2.1. Soil macroporosity and pore size distribution

The total imaged macroporosity ε_{tot} in soil columns was significantly lower in lime treatments compared to controls at Ultuna 3 (Fig. 2a, Table 2), while soils from Ultuna 9 and Oxelby showed no differences between limed and non-limed samples (Fig. 2a, Table 2). The decreases in ε_{tot} after application of lime were associated with shifts in pore size distributions (Fig. 2a). At Ultuna 3, limed soils had significantly smaller macroporosity in the largest size class ($\varepsilon_{>1.0\ mm}$) than the control soils (Fig. 2a, Table 2). These differences in pore volumes between limed and control soils were accompanied by significant differences in the relative contribution of the pore classes to the total imaged porosity. Large macropores contributed relatively less ($\varepsilon_{>1.0\ mm}$) and medium as well as

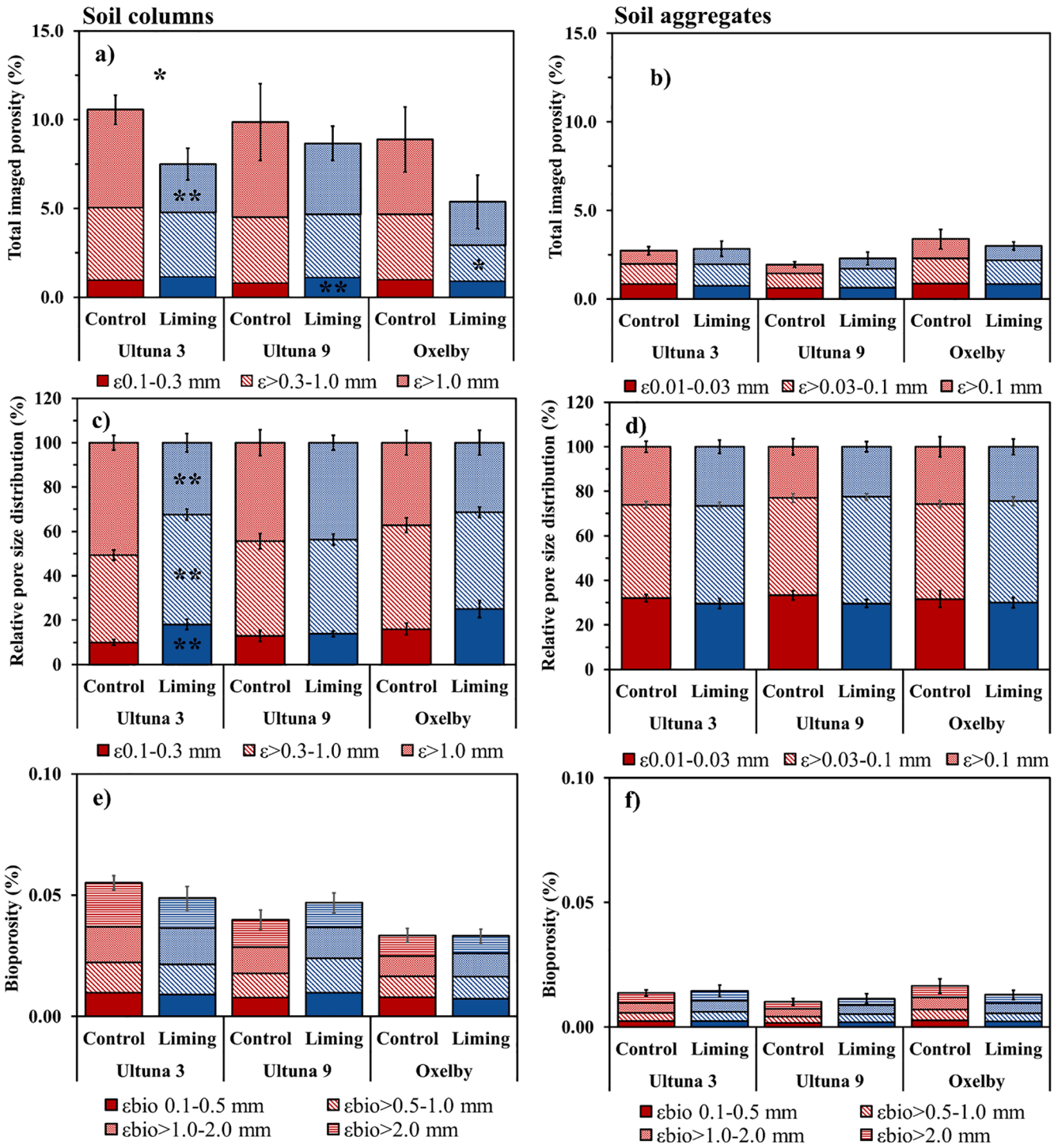

Fig. 2. Soil porosity, pore size distribution, and bioporosity measured on soil columns and aggregates using X-ray CT (50 and 5.5 μm resolution, respectively), comparing lime and control treatments: (a, b) total imaged porosity ε_{tot} and absolute contribution of pore size classes; (c, d) relative pore size distribution; (e, f) total imaged bioporosity ε_{bio} as well as absolute contribution of biopore size classes. Graphs show results for columns (a, c, e; macropores Ø > 0.1 mm) and aggregates (b, d, f; mesopores Ø >0.01 mm). Note the different classification of pore sizes for soil columns, aggregates and biopores. Values displayed as mean (n = 12). Whiskers show standard errors for (a, b) ε_{tot}, (c, d) the different pore size classes, and (e, f) ε_{bio}. Significant differences within field trials are indicated by asterisks (*p < 0.05, **p < 0.01, ***p < 0.001). Indications above bars are for differences in total imaged porosity (ε_{tot}) and indications within bars for differences within pore size classes.

small macropores relatively more (i.e, $\varepsilon_{0.3–1.0\ mm}$ and $\varepsilon_{0.1–0.3\ mm}$, respectively) to the imaged porosity in limed soil compared to controls (Fig. 2c, Table 2). At Ultuna 9 soils had a larger volume of small macropores for limed plots ($\varepsilon_{0.1–0.3\ mm,}$) and at Oxelby, limed soils had a lower absolute volume of medium sized macropores ($\varepsilon_{0.3–1.0\ mm}$; Fig. 2a, Table 2). At both sites, Ultuna 9 and Oxelby, soils showed no differences in relative pore size distribution (Fig. 2 c, Table 2). The analyses of imaged biopores within soil columns did not show any significant differences in bioporosity or in the distribution of biopore size classes between treatments (Fig. 2e, Table 2).

3.2.2. *Macropore architecture and connectivity metrics*

Liming changed the architecture of soil macropores mainly in soils from Ultuna 3 (Fig. 3, Table 2). Macropore networks in soils which

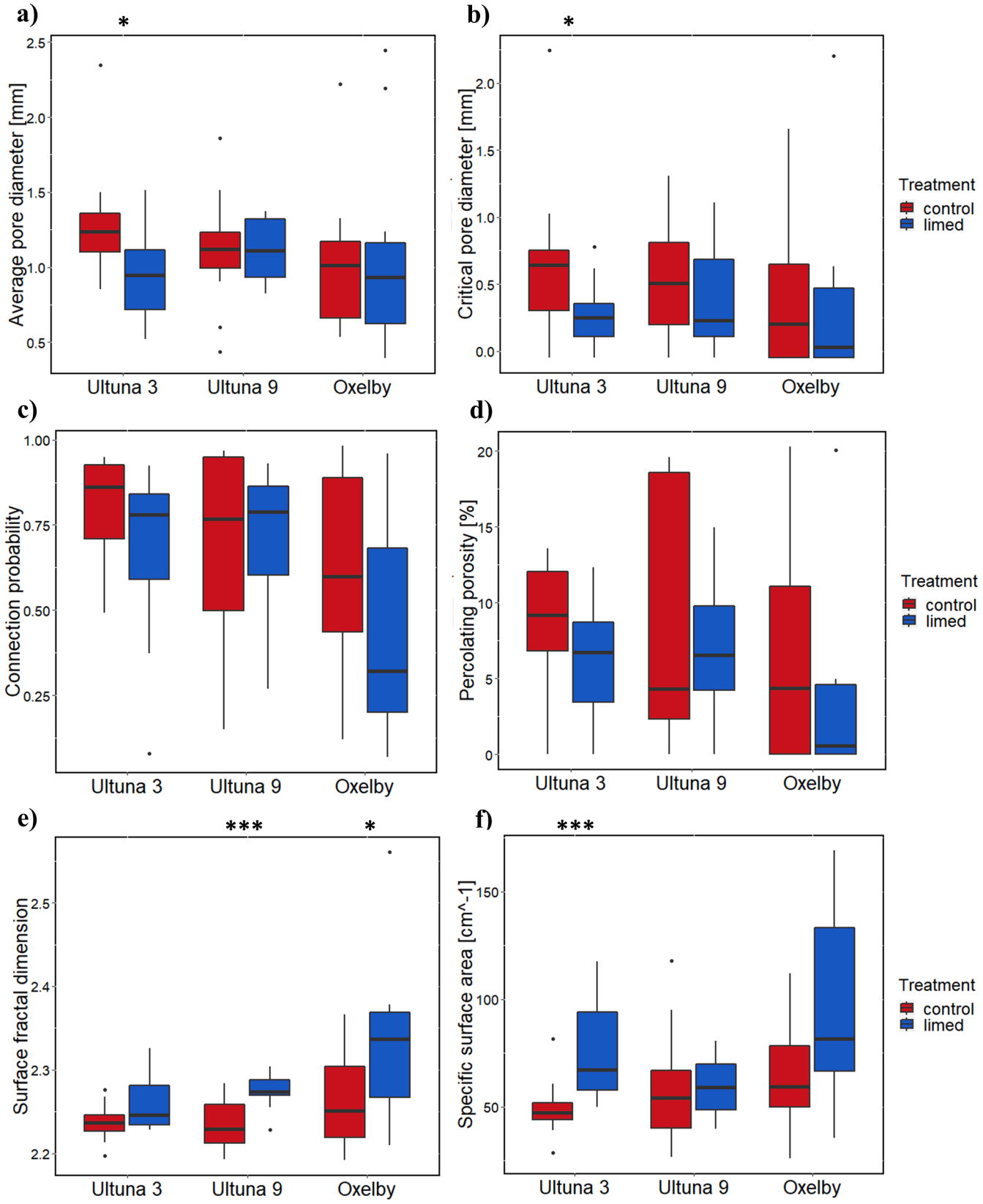

Fig. 3. Macropore (Ø >0.1 mm) architecture and connectivity metrics measured on soil columns using X-ray CT (50 μm resolution), comparing structure lime and control treatments. Boxplots show (a) average pore diameter d_{aver}, (b) critical pore diameter d_{crit}, (c) connection probability Γ, (d) percolating porosity ε_p, (e) surface fractal dimension, and (f) specific surface area. Black dots represent outliers. Significant differences within field trials are indicated by asterisks ($^*p < 0.05$, $^{**}p < 0.01$, $^{***}p < 0.001$) above boxplots.

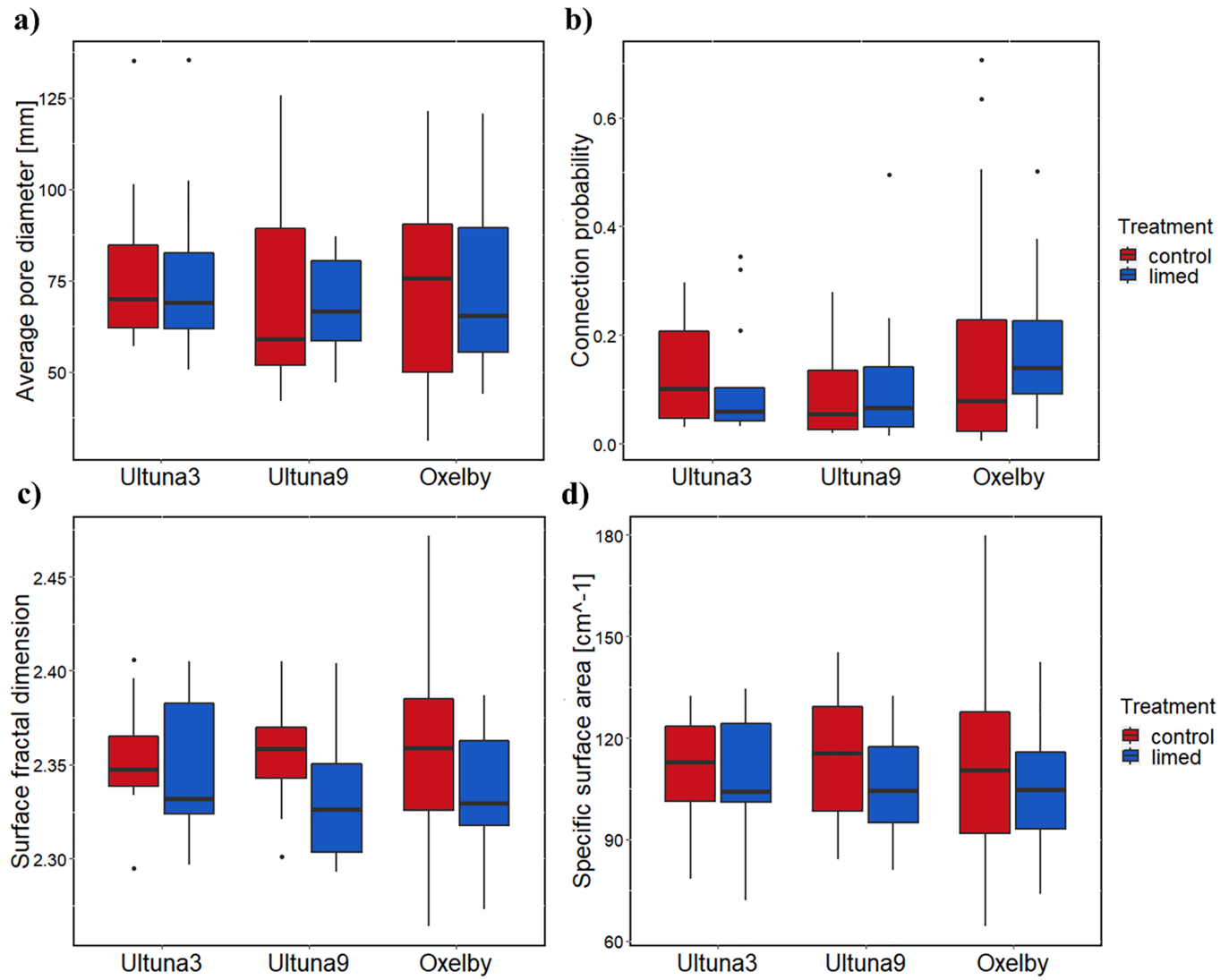

Fig. 4. Mesopore (Ø >0.01 mm) architecture and connectivity metrics measured on soil aggregates using X-ray CT (5.5 µm resolution), comparing structure lime and control treatments. Boxplots show (a) average pore diameter d_{aver}, (b) connection probability Γ, (c) surface fractal dimension, and (d) specific surface area. Black dots represent outliers. Significant differences within field trials are indicated by asterisks (*p < 0.05, **p < 0.01, ***p < 0.001) above boxplots.

Table 3
Size of aggregates obtained for mesopore network analyses (X-ray CT) and readily dispersed soil measured as turbidity values (nephelometric turbidity units, NTU) on soil suspension after wet sieving of additional set of aggregates. Total readily dispersible soil (RDS_{tot}) is based on turbidity measured directly after shaking ($turbidity_{0h}$), readily dispersible clay (RDS_{clay}) is based on turbidity after 4.5 h ($turbidity_{4.5h}$) and readily dispersible soil particles larger than clay ($RDS_{>clay}$) on the difference between $turbidity_{0h}$ and $turbidity_{4.5h}$. Aggregate sizes are mean values ± standard errors (n = 12). Turbidity measures are mean values (n = 16). Asterisks indicate significant differences (*p < 0.05, **p < 0.01, ***p < 0.001).

	Treatment	Aggregate size (mm^3)	RDS_{tot} (NTU)	RDS_{clay} (NTU)	$RDS_{>clay}$ (NTU)
Ultuna 3	limed	163 ± 6	731 *	201 *	530 *
	control	167 ± 5	1381	359	1022
Ultuna 9	limed	148 ± 4	249	76	173
	control	156 ± 6	555	128	427
Oxelby	limed	164 ± 6	173	66	107
	control	167 ± 2	295	100	195

received lime had significantly smaller average (d_{aver}) and critical (d_{crit}) pore diameters at this site (Fig. 3a and b, Table 2). At Ultuna 9 and Oxelby, d_{aver} and d_{crit} were unaffected by liming (Fig. 3a and b, Table 2). The connection probability Γ was similar between lime treated and control soils at all three field sites (Fig. 3c, Table 2). Likewise, the percolating porosity ε_p (i.e. the volume of pore clusters with a connection to the top and bottom of the analysed ROI) showed no differences between limed and control soils at any of the sites (Fig. 3d, Table 2). The surface fractal dimension was affected by liming at two field sites. Soils treated with lime had significantly larger surface fractal dimensions at Ultuna 9 and Oxelby (Fig. 3e, Table 2). The specific surface area of macropores was significantly larger in limed soil compared to control for Ultuna 3, while it was unaffected by lime treatment at Ultuna 9 and Oxelby (Fig. 3f, Table 2).

3.3. Mesopore networks in soil aggregates

Contrary to macropore networks in soil columns, we found no significant differences in any of the measures of total mesopore networks and biopore networks in the soil aggregates (Fig. 2b, d, f; Fig. 4, Table 2).

3.4. Readily dispersible soil

Similar to the pore structure, effects of liming on readily dispersible soil were depending on the field site. At Ultuna 3, all three parameters of readily dispersible soil (i.e. RDS_{tot}, RDS_{clay} and $RDS_{>clay}$) were significantly lower for the limed plots compared to the control plots (Table 2 and 3). At Ultuna 9 and Oxelby no differences in readily dispersible soil occurred between treatments (Table 2 and 3).

4. Discussion

This study provides evidence that structure liming of clay soils can alter soil pore networks and can affect the amounts of readily dispersible soil. Application of structure lime resulted in a decline in macroporosity with shifts from large ($\varepsilon_{>1.0\ mm}$) and medium ($\varepsilon_{0.3–1.0\ mm}$) towards small macropores ($\varepsilon_{0.1–0.3\ mm}$, Fig. 2, Table 2) as well as reduced pore diameters (i.e. d_{aver} and d_{crit}; Fig. 3, Table 2). In contrast, mesopore networks remained unaffected (Figs. 2 and 4, Table 2). Furthermore, liming resulted in reduced amounts of readily dispersible soil (Table 3). The number of parameters with liming-induced modifications differed considerably across the field sites, but the directions of the changes were consistent across sites (Figs. 2 and 3, Table 2 and 3).

4.1. Possible mechanisms behind the observed liming effects on macropore networks

The literature on structure liming describes three mechanism which could have triggered the observed modifications of macropore networks after liming: (i) particle migration due to dispersion (Haynes and Naidu, 1998; Nunes et al., 2018) (ii) pozzolanic reactions (Haynes and Naidu, 1998; Witt, 2002; Zimmermann et al., 2016) and/or (iii) formation of carbonates (Witt, 2002; Zimmermann et al., 2016).

(i) Increasing soil pH can trigger particle dispersion and colloid migration. The mobilized soil particles may be mechanically trapped in pore throats leading to pore clogging (Nunes et al., 2018). Liming induced particle dispersion is, however, short lived (i.e. a few month) and occurs in Al^{3+} rich soils with low pH (i.e. < 5.5) (Haynes and Naidu, 1998). None of these preconditions were fulfilled for the soils in our study (Table 1). In fact, we found that liming tended to reduce the amount of readily dispersible soil (Table 2), making clay dispersion unlikely.

(ii) Pozzolanic reactions can occur in clay soils after quicklime (CaO) or hydrated quicklime ($Ca(OH)_2$) application when the raised pH and electrolyte concentration provoke the dissolution of silicates and aluminates. Silicon and aluminium ions react with calcium leading to the formation of gel-like hydrate phases that may fill pores. With time, these phases cement soil particles together and clog pore networks (Witt, 2002; Zimmermann et al., 2016). Pozzolanic reactions may thus possibly explain the observed decrease in macroporosity ε_{tot} and pore diameters (d_{aver} and d_{crit}) and may have contributed to the reduced amounts of readily dispersible soil for the limed soils. Such changes may have diminished over time in the Oxelby soils, due to the long time period between the end of possible pozzolanic reactions (i.e. they diminish 1–5 years after liming; Witt, 2002; Zimmermann et al., 2016) and soil sampling (i.e. 9–10 years after liming). During this period, soil cultivation and biological activity (see also section 4.3; Haynes and Naidu, 1998; Holland et al., 2018) may have reversed potential alterations in macropore networks. Accordingly, we found only a few liming effects on pore networks for the Oxelby site (Figs. 2 and 3, Table 2). The effects of structure liming on readily dispersible soil that was measured three years after liming at Oxelby (Ulén and Etana, 2014) had vanished.

(iii) Another possible explanation for the altered macropore networks is the formation of carbonates that clog pores. Quicklime (CaO) can react with soil water and CO_2 to form carbonates which form crystals that occupy pore space (Witt, 2002; Zimmermann et al., 2016) in a similar way as hydrate phases.

It is not clear to which extent pozzolanic reactions and formation of carbonates contributed to the observed changes in macropore networks. In our soils, both processes may have occurred simultaneously. However, hydrate phases and carbonates have sizes in the μm scale (Witt, 2002) and it is not clear how they would block pores with much larger sizes. The formation of hydrate phase and carbonates may also have had indirect effects, for instance by keeping pore networks more compacted after soil cultivation due to the cementing of particles. In theory, it is possible to segment carbonate precipitates from the soil matrix in X-ray CT images (i.e. density interval around 2.71 g cm^{-3}), if the precipitates are large enough in relation to the image resolution. However, many soil minerals have densities close to carbonate, making the development of a carbonate segmentation tool for X-ray CT images challenging. Future studies should consider to combine imaging of pore networks by X-ray CT with electron microscopy (Witt, 2002) or synchrotron-based 2D-XANES spectroscopy (Brinza et al., 2014; Monico et al., 2020) on thin sections to investigate the occurrence of hydrate phases and carbonates in relation to pore networks.

4.2. Absence of liming effects on intra-aggregate mesopores

The lack of significant liming effects on mesopore networks was consistent at all field sites (Fig. 2b, d, f, Fig. 4, Table 2). Possibly, concentrations of lime and Ca^{2+} in intra-aggregate mesopores were less affected compared to concentrations in macropores due to transport limitations. Solute transport in intra-aggregate mesopores requires diffusion while transport in inter-aggregate macropores is dominated by advection (Rao et al., 1980; Yang et al., 2014). Because diffusion rates are generally lower than transport rates by advection (Yang et al., 2014), there is more time for Ca^{2+} adsorption (Holland et al., 2018) and/or for chemical reactions that consume Ca^{2+} (Witt, 2002). As a result, lime concentrations within aggregates may not have reached the levels required to cause measurable changes of mesopore architecture.

4.3. Quantitative differences in liming effects between field sites

The liming effects on soil structure and readily dispersible soil differed considerably between field sites. At Ultuna 3, the soil structure was substantially modified by liming, while it was only moderately affected at Ultuna 9 and Oxelby (Figs. 2–4, Table 2). At the latter two field sites, structure lime had apparently no substantial influence on pore networks. However, it is also possible that opposing liming effects may have cancelled each other out. Decreased macroporosity ε_{tot} and pore diameters (d_{aver} and d_{crit}) – mainly found at Ultuna 3 – could have been counterbalanced in soils at Ultuna 9 and Oxelby by the following mechanisms: (i) flocculation and/or (ii) increased biological activity induced by an increase in pH (Table 1; Anikwe et al., 2016; Haynes and Naidu, 1998; Holland et al., 2018). Flocculation of clay-size particles and aggregates occurs after liming in soils with relatively high pH (i.e. pH > 5–6 in $CaCl_2$), because Ca^{2+} increases attractive forces by compressing the diffuse double layer and enables bridging between particles and microaggregates (Haynes and Naidu, 1998). At our field sites, pH in control soils were at the boundary between the two states where liming triggers dispersion on the one hand and flocculation on the other hand (i.e. pH 5.4–6.0 in $CaCl_2$, Table 1). After lime addition, all soils reached pH values where the presence of lime enables flocculation (i.e. pH 6.0–6.7 in $CaCl_2$, Table 1). Flocculation would retain Ca^{2+} which would then not be able to trigger pozzolanic reactions or carbonate formation. It could thus counteract a potential reduction in macroporosity caused by the latter reactions. Flocculation is the opposite of dispersion (Haynes and Naidu, 1998) and may explain the observed reduction in amounts of readily dispersible soil found for Ultuna 3 (Table 3) and for the three years following lime application at Oxelby (Ulén and Etana, 2014). An increase in biological activity could also have counteracted processes which decrease the size and diameter of macropores. Liming can shift soil pH to more favourable conditions for soil biota. Especially the

stimulation of earthworm and root activity can cause increases in macroporosity, while higher activity of other biota mainly increase aggregation and structural stability (Haynes and Naidu, 1998; Holland et al., 2018; Young et al., 1998) and has limited impact on macroporosity (Regelink et al., 2015). Earthworms increase macroporosity through burrowing and roots through growth and subsequent decay. Soil pHs in all control soils were already in a favourable range for roots and earthworms (pH > 5.4, Table 1; Baker and Whitby, 2003) and the analyses of the imaged biopores and their size distribution showed no differences between limed and control soils (Fig. 2e, f). In combination, these two aspects make it unlikely that earthworm or root activity had substantially increased in the limed soils. It leaves flocculation as the most likely liming induced mechanisms which may have counterbalanced the reduction in macroporosity, pore diameters and connection probability.

The limited effects of liming at the Oxelby site may be explained by the long time (9–10 years) between lime application and the analyses carried out in this study. Previous studies indicate that liming effects may vanish within a decade (Holland et al., 2018). Although pH was still significantly higher in limed soil compared to control (Table 1), previously measured effects on readily dispersible soil had disappeared (see section 4.1; Ulén and Etana, 2014). In addition to time, yearly mouldboard ploughing at Oxelby may also have resulted in limited liming effects on soil structure. Auler et al. (2017) found that ploughed soils revealed no differences in porosity after lime application while macroporosity was reduced and pore size distribution shifted towards smaller pores for unploughed soil. Time and soil cultivation can, however, not explain differences in liming effects between the two Ultuna field sites. Both experiments were set up 2–3 years prior to sampling and the management of these sites has been identical (tilled for only 2–3 years using a non-inversion tine cultivator).

The limited effect of structure liming at Ultuna 9 compared to Ultuna 3 may have been due to differences in soil properties. Especially clay and organic matter contents were higher at the Ultuna 9 site (Table 1). Both properties can influence soil structure and amounts of readily dispersible soil (Haynes and Naidu, 1998; Le Bissonnais et al., 1995). In line with the higher content of clay and organic matter, we found that the amount of readily dispersible soil was substantially lower at Ultuna 9 compared to Ultuna 3 (Table 3). At the Ultuna 9 site, the readily dispersible soil was already low before lime application (see control, Table 3). The initially stronger soil structure may explain why liming overall had limited effects at this site. In addition, the applied amount of structure lime may have been too small for the high clay content at Ultuna 9.

4.4. Possible consequences for soil physical processes

The observed changes in macropore networks and structural stability should have consequences for physical processes occurring in the soils. At Ultuna 3, the saturated hydraulic conductivity and aeration is expected to be lower in the limed treatment, because the macroporosity and pore diameters were smaller (Figs. 2 and 3). The consequences of these pore network changes for solute leaching are more uncertain. For high intensity rain storms, which often dominate losses of phosphorous, a reduction in saturated hydraulic conductivity should limit the transport through the limed soil. However, the risk of losses through surface runoff would then increase. For more moderate rainfall events the reduced macroporosity and hydraulic conductivity of limed soil would likely lead to a higher degree of preferential transport since larger pores would be water filled and active in the transport (Koestel et al., 2013; Larsbo et al., 2014).

5. Conclusions

The results of this study show that structure liming of clayey soils can alter macropore networks and reduce the amount of readily dispersible soil, but leaves intra-aggregate mesopore networks unaffected. Liming led to a reduction of total imaged macroporosity mainly by decreasing the amount of larger macropores ($\varepsilon_{>1.0\ mm}$). It further tended to reduce pore diameters. These alterations suggest that structure liming may have deteriorated aeration and reduced saturated hydraulic conductivity, while increasing colloid binding and the potential for preferential macropore flow. The reduction in macroporosity and pore diameters may have been induced by the formation of hydrate phases and carbonates occupying pore space. The changes induced by structure liming were site specific. Only one site (i.e. Ultuna 3) was substantially affected by liming, while the other two sites (i.e. Ultuna 9 and Oxelby) showed only few liming-induced changes. The reasons for the limited liming effects at the latter two sites could not be revealed. However, at Oxelby yearly ploughing in combination with the long period between lime application and our analyses may be the main reason. It is not possible to draw any firm conclusions from our results on how and by which processes liming would influence leaching of strongly sorbing compounds like phosphorous. To separate effects of liming on pore networks from effects on particle facilitated transport, future studies should combine X-ray tomography of macropore networks and analysis of readily dispersible soil with transport experiments for both reactive and non-reactive compounds.

Funding

This work was supported by the Swedish Research Council Formas (Grant nr: 2013-609).

Declaration of Competing Interest

The authors declare that they have no known competing financial interests or personal relationships that could have appeared to influence the work reported in this paper.

Acknowledgments

The authors thank Farid Jan at the Dept. Soil and Environment, SLU, for support with pH measurements.

References

Almajmaie, A., Hardie, M., Acuna, T., Birch, C., 2017. Evaluation of methods for determining soil aggregate stability. Soil Tillage Res. 167, 39–45. https://doi.org/10.1016/j.still.2016.11.003.

Ananyeva, K., Wang, W., Smucker, A.J.M., Rivers, M.L., Kravchenko, A.N., 2013. Can intra-aggregate pore structures affect the aggregate's effectiveness in protecting carbon? Soil Biol. Biochem. 57, 868–875. https://doi.org/10.1016/j.soilbio.2012.10.019.

Anikwe, M.A.N., Eze, J.C., Ibudialo, A.N., 2016. Influence of lime and gypsum application on soil properties and yield of cassava (Manihot esculenta Crantz.) in a degraded Ultisol in Agbani, Enugu Southeastern Nigeria. Soil Tillage Res. 158, 32–38. https://doi.org/10.1016/j.still.2015.10.011.

Auler, A.C., Pires, L.F., dos Santos, J.A.B., Caires, E.F., Borges, J.A.R., Giarola, N.F.B., 2017. Effects of surface-applied and soil-incorporated lime on some physical attributes of a Dystrudept soil. Soil Use Manage. 33, 129–140. https://doi.org/10.1111/sum.12330.

Baker, G.H., Whitby, W.A., 2003. Soil pH preferences and the influences of soil type and temperature on the survival and growth of Aporrectodea longa (Lumbricidae). Pedobiologia 47, 745–753. https://doi.org/10.1078/0031-4056-00254.

Berglund, G., 1971. Kalkens inverkan på jordens struktur. Grundförbättring 24, 81–93.

Berglund, K., Etana, A., Simonsson, M., 2017. EKOKALK: Strukturkalkning för förbättrad markstruktur och minskade fosforförluster i ekologisk odling? Jönköping, Sweden.

Blomquist, J., Simonsson, M., Etana, A., Berglund, K., 2018. Structure liming enhances aggregate stability and gives varying crop responses on clayey soils. Acta Agric. Scand. Sect. B Soil Plant Sci. 68, 311–322. https://doi.org/10.1080/09064710.2017.1400096.

Brinza, L., Schofield, P.F., Hodson, M.E., Weller, S., Ignatyev, K., Geraki, K., Quinn, P.D., Mosselmans, J.F.W., 2014. Combining μxANES and μxRD mapping to analyse the heterogeneity in calcium carbonate granules excreted by the earthworm Lumbricus terrestris. J. Synchrotron Radiat. 21, 235–241. https://doi.org/10.1107/S160057751303083X.

Bronick, C.J., Lal, R., 2005. Soil structure and management: A review. Geoderma 124, 3–22. https://doi.org/10.1016/j.geoderma.2004.03.005.

Carmeis Filho, A.C.A., Crusciol, C.A.C., Guimarães, T.M., Calonego, J.C., Mooney, S.J., 2016. Impact of amendments on the physical properties of soil under tropical long-

term no till conditions. PLoS ONE 11 (12), e0167564. https://doi.org/10.1371/journal.pone.0167564.
Chan, K.Y., Conyers, M.K., Scott, B.J., 2007. Improved structural stability of an acidic hardsetting soil attributable to lime application. Commun. Soil Sci. Plant Anal. 38, 2163–2175. https://doi.org/10.1080/00103620701549108.
Choquette, M., Bérubé, M.-A., Locat, J., 1987. Mineralogical and Microtextural Changes Associated with Lime Stabilization of Marine Clays from Eastern Canada. Appl. Clay Sci. 2, 215–232.
Climate-Data.org, 2020. Klimat Södertälje (Sverige). URL https://sv.climate-data.org/europa/sverige/stockholms-laen/soedertaelje-9496/ (accessed 6.9.20).
Czyż, E.A., Dexter, A.R., 2015. Mechanical dispersion of clay from soil into water: readily-dispersed and spontaneously-dispersed clay. Int. Agrophys. 29, 31–37. https://doi.org/10.1515/intag-2015-0007.
Dexter, A.R., 1988. Advances in characterization of soil structure. Soil Tillage Res. 11, 199–238. https://doi.org/10.1016/0167-1987(88)90002-5.
Doube, M., Klosowski, M.M., Arganda-Carreras, I., Cordelières, F.P., Dougherty, R.P., Jackson, J.S., Schmid, B., Hutchinson, J.R., Shefelbine, S.J., 2010. BoneJ: Free and extensible bone image analysis in ImageJ. Bone 47, 1076–1079. https://doi.org/10.1016/j.bone.2010.08.023.
Dougherty, R.P., Kunzelmann, K.-H., 2007. Computing local thickness of 3D structures with ImageJ. Microsc. Microanal. 13, 1678–1679. https://doi.org/10.1017/S1431927607074430.
FAO, 1998. World reference base for soil resources. Food and Agriculture Organization of the United Nations, Rome.
Ferreira, T.R., Pires, L.F., Wildenschild, D., Brinatti, A.M., Borges, J.A.R., Auler, A.C., dos Reis, A.M.H., 2019. Lime application effects on soil aggregate properties: Use of the mean weight diameter and synchrotron-based X-ray μCT techniques. Geoderma 338, 585–596. https://doi.org/10.1016/j.geoderma.2018.10.035.
Ferreira, T.R., Pires, L.F., Wildenschild, D., Heck, R.J., Antonino, A.C.D., 2018. X-ray microtomography analysis of lime application effects on soil porous system. Geoderma 324, 119–130. https://doi.org/10.1016/j.geoderma.2018.03.015.
Gee, G.W., Or, D., 2002. 2.4 Particle-size analysis. In: Dane, J.H., Topp, G.C. (Eds.), Methods of Soil Analysis: Part 4 Physical Methods, 5.4. Soil Science Society of America, Inc., Madison, WI, USA, pp. 255–293.
Grieve, I.C., Davidson, D.A., Bruneau, P.M.C., 2005. Effects of liming on void space and aggregation in an upland grassland soil. Geoderma 125, 39–48. https://doi.org/10.1016/j.geoderma.2004.06.004.
Haynes, R.J., Naidu, R., 1998. Influence of lime, fertilizer and manure applications on soil organic matter content and soil physical conditions: a review. Nutr. Cycl. Agroecosyst. 51, 123–137. https://doi.org/10.1023/A:1009738307837.
Helliwell, J.R., Sturrock, C.J., Grayling, K.M., Tracy, S.R., Flavel, R.J., Young, I.M., Whalley, W.R., Mooney, S.J., 2013. Applications of X-ray computed tomography for examining biophysical interactions and structural development in soil systems: A review. Eur. J. Soil Sci. 64, 279–297. https://doi.org/10.1111/ejss.12028.
Hellner, Q., Koestel, J., Ulén, B., Larsbo, M., 2018. Effects of tillage and liming on macropore networks derived from X-ray tomography images of a silty clay soil. Soil Use Manage. 34, 197–205. https://doi.org/10.1111/sum.12418.
Holland, J.E., Bennett, A.E., Newton, A.C., White, P.J., McKenzie, B.M., George, T.S., Pakeman, R.J., Bailey, J.S., Fornara, D.A., Hayes, R.C., 2018. Liming impacts on soils, crops and biodiversity in the UK: A review. Sci. Total Environ. 610–611, 316–332. https://doi.org/10.1016/j.scitotenv.2017.08.020.
Keiblinger, K.M., Bauer, L.M., Deltedesco, E., Holawe, F., Unterfrauner, H., Zehetner, F., Peticzka, R., 2016. Quicklime application instantly increases soil aggregate stability. Int. Agrophys. 30, 123–128. https://doi.org/10.1515/intag-2015-0068.
Kittler, J., Illingworth, J., 1986. Minimum error thresholding. Pattern Recognit. 19, 41–47.
Koestel, J., 2018. SoilJ: An ImageJ plugin for the semiautomatic processing of three-dimensional X-ray images of soils. Vadose Zo. J. 17, 1–7. https://doi.org/10.2136/vzj2017.03.0062.
Koestel, J., Larsbo, M., 2014. Imaging and quantification of preferential solute transport in soil macropores. Water Resour. Res 50, 4357–4378. https://doi.org/10.1002/2014WR015351.
Koestel, J., Schlüter, S., 2019. Quantification of the structure evolution in a garden soil over the course of two years. Geoderma 338, 597–609. https://doi.org/10.1016/j.geoderma.2018.12.030.
Koestel, J.K., Norgaard, T., Luong, N.M., Vendelboe, A.L., Moldrup, P., Jarvis, N.J., Lamandé, M., Iversen, B.V., Wollesen De Jonge, L., 2013. Links between soil properties and steady-state solute transport through cultivated topsoil at the field scale. Water Resour. Res. 49, 790–807. https://doi.org/10.1002/wrcr.20079.
Larsbo, M., Koestel, J., Jarvis, N., 2014. Relations between macropore network characteristics and the degree of preferential solute transport. Hydrol. Earth Syst. Sci. 18, 5255–5269. https://doi.org/10.5194/hess-18-5255-2014.
Le Bissonnais, Y., Renaux, B., Delouche, H., 1995. Interactions between soil properties and moisture content in crust formation, runoff and interrill erosion from tilled loess soils. Catena 25, 33–46. https://doi.org/10.1016/0341-8162(94)00040-L.
Legland, D., Arganda-Carreras, I., Andrey, P., 2016. MorphoLibJ: Integrated library and plugins for mathematical morphology with ImageJ. Bioinformatics 32, 3532–3534. https://doi.org/10.1093/bioinformatics/btw413.
Longair, M., Preibisch, S., Tinevez, J.-Y., 2017. Tubness (ImageJ). URL https://imagej.net/Tubeness (accessed 5.15.20).
Lucas, M., Schlüter, S., Vogel, H.J., Vetterlein, D., 2019. Soil structure formation along an agricultural chronosequence. Geoderma 350, 61–72. https://doi.org/10.1016/j.geoderma.2019.04.041.
Monico, L., Cartechini, L., Rosi, F., De Nolf, W., Cotte, M., Vivani, R., Maurich, C., Miliani, C., 2020. Synchrotron radiation Ca K-edge 2D-XANES spectroscopy for studying the stratigraphic distribution of calcium-based consolidants applied in limestones. Sci. Rep. 10, 14337. https://doi.org/10.1038/s41598-020-71105-8.
Nunes, M.R., Vaz, C.M.P., Denardin, J.E., van Es, H.M., Libardi, P.L., da Silva, A.P., 2018. Physicochemical and structural properties of an oxisol under the addition of straw and lime. Soil Sci. Soc. Am. J. 81, 1328. https://doi.org/10.2136/sssaj2017.07.0218.
Perret, J.S., Prasher, S.O., Kacimov, A.R., 2003. Mass fractal dimension of soil macropores using computed tomography: From the box-counting to the cube-counting algorithm. Eur. J. Soil Sci. 54, 569–579. https://doi.org/10.1046/j.1365-2389.2003.00546.x.
Prewitt, J.M.S., Mendelsohn, M.L., 1966. The analysis of cell images. Ann. N. Y. Acad. Sci. 128, 1035–1053. https://doi.org/10.1111/j.1749-6632.1965.tb11715.x.
Rao, P.S.C., Rolston, D.E., Jessup, R.E., Davidson, J.M., 1980. Solute transport in aggregated porous media: theoretical and experimental evaluation. Soil Sci. Soc. Am. J. 44, 1139–1146. https://doi.org/10.2136/sssaj1980.03615995004400060003x.
Regelink, I.C., Stoof, C.R., Rousseva, S., Weng, L., Lair, G.J., Kram, P., Nikolaidis, N.P., Kercheva, M., Banwart, S., Comans, R.N.J., 2015. Linkages between aggregate formation, porosity and soil chemical properties. Geoderma 247–248, 24–37. https://doi.org/10.1016/j.geoderma.2015.01.022.
Renard, P., Allard, D., 2013. Connectivity metrics for subsurface flow and transport. Adv. Water Resour. 51, 168–196. https://doi.org/10.1016/j.advwatres.2011.12.001.
Rodrigues da Silva, F., Albuquerque, J.A., da Costa, A., Fontoura, S.M.V., Bayer, C., Warmling, M.I., 2016. Physical properties of a hapludox after three decades under different soil management systems. Rev. Bras. Cienc. do Solo 40, 1–14. https://doi.org/10.1590/18069657rbcs20140331.
Sandin, M., Koestel, J., Jarvis, N., Larsbo, M., 2017. Post-tillage evolution of structural pore space and saturated and near-saturated hydraulic conductivity in a clay loam soil. Soil Tillage Res. 165, 161–168. https://doi.org/10.1016/j.still.2016.08.004.
Schindelin, J., Arganda-Carreras, I., Frise, E., Kaynig, V., Longair, M., Pietzsch, T., Preibisch, S., Rueden, C., Saalfeld, S., Schmid, B., Tinevez, J.Y., White, D.J., Hartenstein, V., Eliceiri, K., Tomancak, P., Cardona, A., 2012. Fiji: An open-source platform for biological-image analysis. Nat. Methods 9, 676–682. https://doi.org/10.1038/nmeth.2019.
Schneider, C.A., Rasband, W.S., Eliceiri, K.W., 2012. NIH Image to ImageJ: 25 years of image analysis. Nat. Methods 9, 671–675. https://doi.org/10.1038/nmeth.2089.
Shanmuganathan, R.T., Oades, J.M., 1983. Modification of soil physical properties by addition of calcium compounds. Aust. J. Soil Res. 21, 285–300.
Sheldrick, B.H., Wang, C., 1993. Particle Size Distribution. In: Carter, M.R. (Ed.), Soil Sampling and Methods of Analysis. CRC Press, Boca Raton, FL, USA, pp. 499–511.
Svanbäck, A., Ulén, B., Etana, A., 2014. Mitigation of phosphorus leaching losses via subsurface drains from a cracking marine clay soil. Agric. Ecosyst. Environ. 184, 124–134. https://doi.org/10.1016/j.agee.2013.11.017.
Ulén, B., Alex, G., Kreuger, J., Svanbäck, A., Etana, A., 2012. Particulate-facilitated leaching of glyphosate and phosphorus from a marine clay soil via tile drains. Acta Agric. Scand. Sect. B Soil Plant Sci. 62, 241–251. https://doi.org/10.1080/09064710.2012.697572.
Ulén, B., Etana, A., 2014. Phosphorus leaching from clay soils can be counteracted by structure liming. Acta Agric. Scand. Sect. B Soil Plant Sci. 64, 425–433. https://doi.org/10.1080/09064710.2014.920043.
Ulén, B., Persson, K., 1999. Field-scale phosphorus losses from a drained clay soil in Sweden. Hydrol. Process. 13, 2801–2812. https://doi.org/10.1002/(SICI)1099-1085(19991215)13:17<2801::AID-HYP900>3.0.CO;2-G.
Wang, W., Kravchenko, A.N., Smucker, A.J.M., Liang, W., Rivers, M.L., 2012. Intra-aggregate Pore Characteristics: X-ray Computed Microtomography Analysis. Soil Sci. Soc. Am. J. 76, 1159–1171. https://doi.org/10.2136/sssaj2011.0281.
Wiklander, L., 1963. Kalkens betydelse för markens struktur. In: Svenskt Jordbruk Och Skogsbruk 1913–1962. Kungl. Skogs- och Lantbruksakademien, Stockholm, pp. 249–259.
Wiklander, L., Lotse, E., 1966. Mineralogical and physico-chemical studies on clay fractions of Swedish cultivated soils. Lantbrukshogskolns Ann. 32, 139–415.
Witt, K.J., 2002. Zement - Kalk - Stabilisierung von Böden. Schriftenr. Geotech, Weimar Heft, p. 7.
Yang, X., Richmond, M.C., Scheibe, T.D., Perkins, W.A., Resat, H., 2014. Flow partitioning in fully saturated soil aggregates. Transp. Porous Media 103, 295–314. https://doi.org/10.1007/s11242-014-0302-y.
Young, I.M., Blanchart, E., Chenu, C., Dangerfield, M., Fragoso, C., Grimaldi, M., Ingram, J., Monrozier, L.J., 1998. The interaction of soil biota and soil structure under global change. Glob. Chang. Biol. 4, 703–712. https://doi.org/10.1046/j.1365-2486.1998.00194.x.
Zimmermann, I., Fleige, H., Horn, R., 2016. Soil structure amelioration with quicklime and irrigation experiments in earth graves. J. Soils Sediments 16, 2514–2522. https://doi.org/10.1007/s11368-016-1509-z.